Vector fitting approximation of a cylinder nonreflecting boundary kernel

K. Bavelis and C. Mias

To employ the modal nonreflecting boundary condition (MNRBC) in cylindrical coordinates in the finite element time domain (FETD) method, a time domain kernel expression must be found that it is the inverse Laplace transform (ILT) of a known frequency domain function. The inverse Laplace transformation is achieved using a methodology based on the partial fraction expansion of the frequency domain function. However, to date, no FETD results have been published based on this MNRBC methodology. A simpler implementation of the methodology based on vector fitting (VF) is proposed. Using the VF approach, FETD-MNRBC results of plane wave scattering from a cylinder are presented for the first time.

Introduction: The modal nonreflecting boundary condition (MNRBC), in cylindrical coordinates, is a well established boundary condition in the two-dimensional (2D) finite element frequency domain (FEFD) method simulations [1]. This boundary condition is based on the fact that the scattered field on a circular (fictitious) boundary surrounding a cylinder of arbitrary cross-section can be expressed in terms of summation of modal functions, of integer modal orders *n*, which are products of Hankel functions or modified Bessel functions and azimuthal function terms, see for example [2]. The time domain version of this boundary condition has not been employed in finite element time domain (FETD) method simulations although the general methodology for developing a time domain MNRBC has been presented by Alpert et al [3]. The methodology relies on finding, for each order *n*, the time domain expression of a cylinder nonreflecting boundary kernel. This requires that for each order *n* the inverse Laplace transform (ILT) of a known function that appears in the MNRBC in the frequency domain is found. This is achieved by expressing the frequency domain function as a summation of partial fractions which via the ILT are expressed as a summation of exponential terms in the time domain. Because of the complexity involved in implementing the partial fraction expansion in [3] and the fact that only a limited number of partial fraction coefficients that correspond to a few cylinder kernel modal orders (n =1,2,3,4) were presented in [3], an alternative simpler approach of implementing the partial fraction expansion based on vector fitting (VF) is proposed using the publicly available software VECTFIT [4]. This VF approach may have a greater appeal among engineers. Through computations, it is demonstrated that the VF results are of comparable accuracy to those of Alpert et al [3]. In addition, FETD-MNRBC results, based on VF, are presented for the first time.

The VF approach: To demonstrate the proposed VF partial fraction expansion approach and its accuracy, the Laplace transform expression $Q_n(s)$ of the time domain cylinder nonreflecting boundary kernel $q_n(t)$, used by Alpert et al (eq. 2.13 in [3]), is employed

$$Q_n(s) = \frac{s}{c} + \frac{1}{2\rho} + \frac{s}{c}\frac{K'_n(\rho s/c)}{K_n(\rho s/c)} = \frac{1}{\rho}\left[v + \frac{1}{2} + v\frac{K'_n(v)}{K_n(v)}\right], \quad v = \frac{s\rho}{c} \tag{1}$$

where K_n is the modified Bessel function of the second kind and nth order. The derivative K'_n of K_n is with respect to the argument $\rho s/c$ where s is the Laplace domain variable, ρ is the radius of the fictitious circular nonreflecting boundary ($\rho > 0$), c is the speed of light in the medium surrounding the cylinder ($c > 0$), assumed here to be free space. From the scaling properties of the Laplace transform it is sufficient to expand the following expression in terms of partial functions

$$U_n(s) = s + \frac{1}{2} + s\frac{K'_n(s)}{K_n(s)} = s + \frac{1}{2} - s\frac{K_{n+1}(s)}{K_n(s)} + n \tag{2}$$

In (2), the derivative K'_n of K_n is now with respect to the argument s. Once the ILT of $U_n(s)$ is found, denoted as $u_n(t)$, then the ILT of (1) can be obtained, for any ρ and c, as follows

$$q_n(t) = \frac{c}{\rho^2} u_n\left(\frac{c}{\rho}t\right) \tag{3}$$

The last expression in (2) is obtained using the identities of modified Bessel functions in [5] and it is the expression employed in VF with $s = j\omega$. In general, VF approximately expresses $U_n(s)$ in (2) in the following form

$$U_n(s) \approx U_{n,app}(s) = d_n + h_n s + \sum_{m=1}^{M} \frac{r_{m,n}}{s - a_{m,n}} \tag{4}$$

where the parameters d_n, h_n, $r_{m,n}$ (pole coefficient) and $a_{m,n}$ (pole location) are computed by VECTFIT (version 1). The subscript '*app*' indicates an approximation. To enable VECTFIT to produce the desirable results, the asymptotic value of $U_n(s)$ as $s \to 0$ is required. From [5], the small argument approximation of $U_n(s)$ is

$$\lim_{s \to 0} U_n(s) \approx \frac{1}{2} - |n| \quad \forall\, n \in \mathbf{Z} \quad \text{since} \quad \lim_{s \to 0} K_n(s) \approx \frac{1}{2}\Gamma(n)\left(\frac{1}{2}s\right)^{-n} \ \text{for } n > 0 \tag{5}$$

where $\Gamma(\ldots)$ is the Gamma function [5]. Furthermore, computing d_n and h_n is optional in VECTFIT and therefore knowledge of the large argument approximation of $U_n(s)$ is beneficial. In this case, $U_n(s) \to 0$ as $s \to \infty$, hence, $d_n = h_n = 0$. Therefore, after applying ILT to the partial fraction expansion in (4) one obtains the following approximate time domain expression for $u_n(t)$,

$$u_{n,app}(t) = \sum_{m=1}^{M} r_{m,n} e^{a_{m,n} t} \tag{6}$$

A benefit from employing such a summation in a FETD-MNRBC formulation is that it will allow the convolution that appears in the boundary integral term of the formulation to be computed in a fast manner using a recursive approach as shown in [6] for 2D planar periodic structures.

Numerical Results: The input parameters used in VECTFIT were: (a) 4000 frequency samples; (b) a frequency range of $0 \le f \le f_{max}$ with $f_{max} = 4$ Hz; (c) iter = 20 iterations; and (d) asympflag = 1 (as $d_n = h_n = 0$). Table 1 lists the computed partial fraction parameters, $r_{m,n}$ and $a_{m,n}$. Their values are truncated to six decimal places. For n and M the values tabulated in [3] are used. Figure 1 shows plots of the function $U_n(s = j2\pi f)$ versus frequency f based on: (a) the exact equation (2);

(b) the partial fraction approximation of the VF using the parameters in table 1 (without truncation); and (c) the partial fraction approximation of Alpert et al using the tabulated parameters in [3]. The absolute error value $10\log_{10}|e_n(s = j2\pi f)|$ versus frequency f is also shown in figure 1 for both approximations, where

$$|e_n(s)| = \left| U_n(s) - \sum_{m=1}^{M} \frac{r_{m,n}}{s - a_{m,n}} \right| \tag{7}$$

The figure indicates that both approximations are of comparable accuracy and that $10\log_{10}|e_n| < -50$ dB for $n = 1,2,3,4$.

The VF accuracy enabled us to obtain, for the first time, FETD-MNRBC results (figure 2) based on the proposed VF approach. The plot in figure 2 shows the bistatic scattering width ($\sigma_{2\text{-D}}/\lambda$), as defined in [7], of a perfectly electrically conducting triangular cylinder. The cylinder is surrounded by free space. The FETD-MNRBC results are compared with the integral equation formulation results presented in [2].

Conclusion: A VF approximation of a cylinder nonreflecting boundary kernel is proposed and validated. FETD-MNRBC results, based on this VF approximation, are presented for the first time.

References

1 JENG, S.K., and CHEN, C.H. : 'On Variational Electromagnetics: Theory and Application', IEEE Transactions on Antennas and Propagation, 1984, 32, (9), pp. 902-907

2 PETERSON, A.F., and CASTILLO, S.P. : 'A Frequency-Domain Differential Equation Formulation for Electromagnetic Scattering from Inhomogeneous Cylinders' , IEEE Transactions on Antennas and Propagation, 1989, 37, (5), pp. 601-607

3 ALPERT, B., GREENGARD, L., and HAGSTROM, T. : 'Rapid evaluation of nonreflecting boundary kernels for time-domain wave propagation', SIAM Journal on Numerical Analysis, 2000, 37, (4), pp. 1138–1164

4 GUSTAVSEN, B., SEMLYEN, A., : 'Rational Approximation of Frequency Domain Responses by Vector Fitting', IEEE Transactions on Power Delivery, 1999, 14, (3), pp. 1052-1061

5 ABRAMOWITZ, M., and STEGUN, I.A. : 'Handbook of Mathematical Functions: With Formulas, Graphs, and Mathematical Tables' (Dover Publications, New York, 1965)

6 CAI, Y., and MIAS, C. : 'Fast Finite Element Time Domain – Floquet Absorbing Boundary Condition modelling of periodic structures using recursive convolution', IEEE Transactions on Antennas and Propagation, 2007, 55, (9), pp. 2550-2558

7 BALANIS, C.A. : 'Advanced Engineering Electromagnetics' (Wiley, New York, 1989)

Authors' affiliations:

K. Bavelis and C. Mias (School of Engineering, Warwick University, Coventry, CV4 7AL, United Kingdom)

Corresponding author email address: K.Bavelis@warwick.ac.uk

Figure and Table Captions

Figure 1

Caption:

Plots of $|U_n(s = j2\pi f)|$ and $10\log_{10}|e_n(s = j2\pi f)|$ versus frequency f for $n = 1,2,3,4$.

Figure 2

Caption:

Bistatic scattering width, $10\log_{10}(\sigma_{2\text{-D}}/\lambda)$, of a triangular cylinder. $x_1 = 1.0\lambda$, $x_2 = -0.707\lambda$, $y_1 = 0.707\lambda$ and $y_2 = -y_1$. For simplicity, $\lambda = 1$ m . The incident plane wave, with the electric field vector in the z-direction, is propagating in the negative x-direction. Surface Ω represents the finite element region and Γ represents the circular boundary on which the MNRBC is applied.

Table 1

Caption:

VF computed parameters

Figure 1

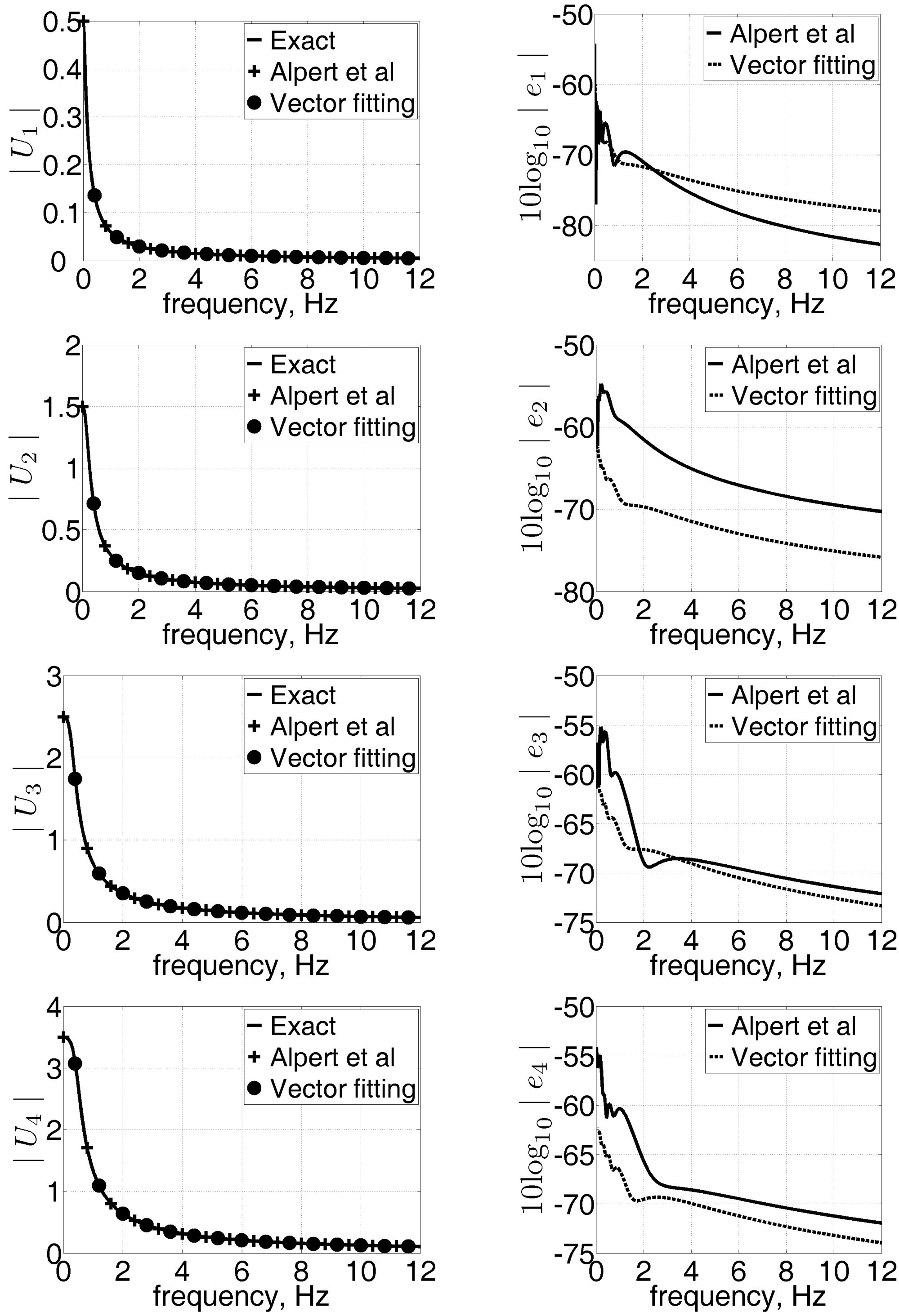
Exact
Alpert et al
Vector fitting
$|U_1|$
$|U_2|$
$|U_3|$
$|U_4|$
$10\log_{10}|e_1|$
$10\log_{10}|e_2|$
$10\log_{10}|e_3|$
$10\log_{10}|e_4|$
frequency, Hz

Figure 2

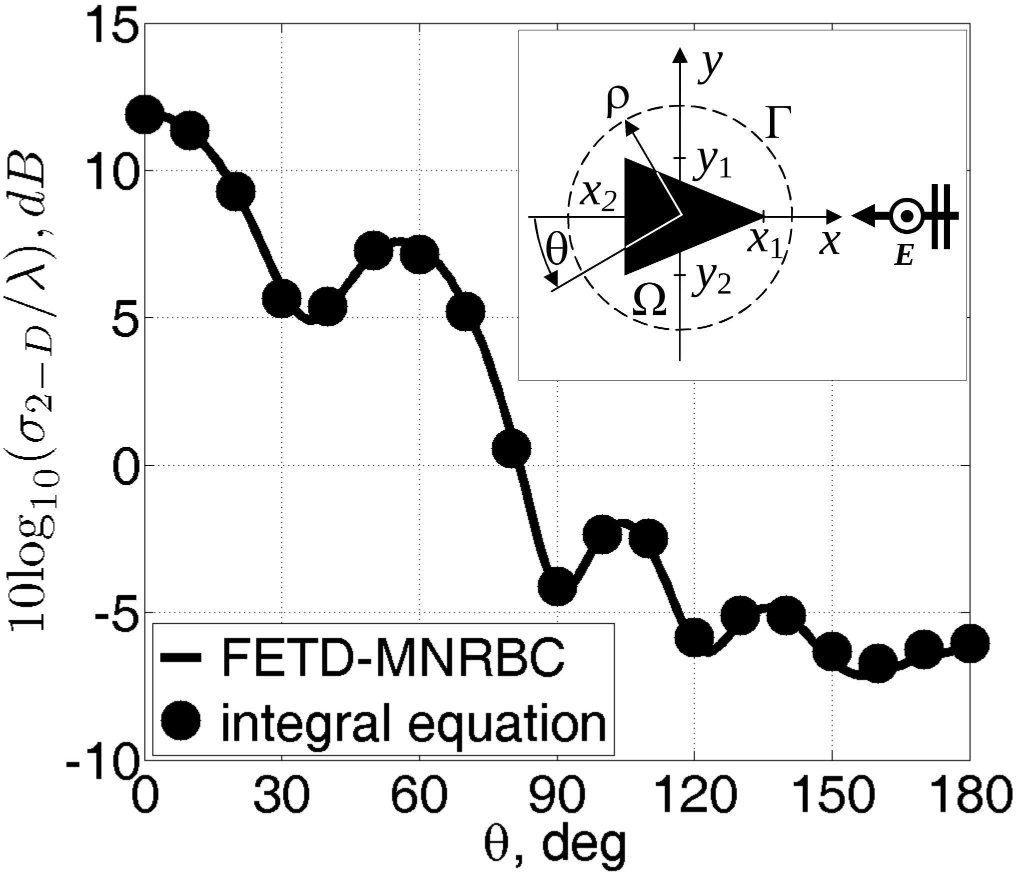

15
10
5
0
-5
-10
0
30
60
90
120
150
180
θ, deg
$10\log_{10}(\sigma_{2-D}/\lambda), dB$
FETD-MNRBC
integral equation
y
ρ
Γ
y_1
x_2
θ
x_1
x
y_2
Ω
E

Table 1

n	M	Pole coefficients		Pole locations	
		Real	Imaginary	Real	Imaginary
1	9	-6.125650×10^{-3}	0	-3.465994×10^{0}	0
		-5.259487×10^{-2}	0	-1.904945×10^{0}	0
		-1.381366×10^{-1}	0	-1.091376×10^{0}	0
		-1.326909×10^{-1}	0	-6.548468×10^{-1}	0
		-3.918820×10^{-2}	0	-3.765733×10^{-1}	0
		-5.643938×10^{-3}	0	-1.921838×10^{-1}	0
		-5.779033×10^{-4}	0	-8.671415×10^{-2}	0
		$-3.945792 \cdot \times 10^{-5}$	0	-3.308866×10^{-2}	0
		-1.182999×10^{-6}	0	-8.940158×10^{-3}	0
2	6	2.087022×10^{-4}	0	-2.352687×10^{-1}	0
		1.883591×10^{-2}	0	-6.004027×10^{-1}	0
		9.779644×10^{-1}	0	-1.585323×10^{0}	0
		2.405753×10^{-2}	0	-3.281031×10^{0}	0
		-1.448034×10^{0}	1.672191×10^{-1}	-1.261094×10^{0}	4.080800×10^{-1}
		-1.448034×10^{0}	-1.672191×10^{-1}	-1.261094×10^{0}	-4.080800×10^{-1}
3	5	-1.096578×10^{-2}	0	-9.316772×10^{-1}	0
		-7.920391×10^{-1}	0	-1.852993×10^{0}	0
		-1.997077×10^{-1}	0	-3.049055×10^{0}	0
		-1.686141×10^{0}	1.291524×10^{0}	-1.680029×10^{0}	1.307535×10^{0}
		-1.686141×10^{0}	-1.291524×10^{0}	-1.680029×10^{0}	-1.307535×10^{0}
4	5	3.742610×10^{-1}	0	-1.975139×10^{0}	0
		-2.148009×10^{0}	1.917512×10^{0}	-2.813927×10^{0}	4.063061×10^{-1}
		-2.148009×10^{0}	-1.917512×10^{0}	-2.813927×10^{0}	-4.063061×10^{-1}
		-1.976622×10^{0}	2.208657×10^{0}	-1.978586×10^{0}	2.204506×10^{0}
		-1.976622×10^{0}	-2.208657×10^{0}	-1.978586×10^{0}	-2.204506×10^{0}